Photodissociation of the OD radical at 226 and 243 nm

Dragana Č. Radenović, André J. A. van Roij, Dmitri A. Chestakov, André T. J. B. Eppink, J. J. ter Meulen, and David H. Parker[a)]
Department of Molecular and Laser Physics, University of Nijmegen, Toernooiveld 1, 6525ED, Nijmegen, The Netherlands

Mark P. J. van der Loo and Gerrit C. Groenenboom
Institute of Theoretical Chemistry, University of Nijmegen, Toernooiveld 1, 6525ED, Nijmegen, The Netherlands

Margaret E. Greenslade and Marsha I. Lester
Department of Chemistry, University of Pennsylvania, Philadelphia, Pennsylvania 19104-6323

(Received 28 August 2003; accepted 11 September 2003)

The photodissociation dynamics of state selected OD radicals has been examined at 243 and 226 nm using velocity map imaging to probe the angle–speed distributions of the $D(^2S)$ and $O(^3P_2)$ products. Both experiment and complementary first principle calculations demonstrate that photodissociation occurs by promotion of OD from high vibrational levels of the ground $X\ ^2\Pi$ state to the repulsive $1\ ^2\Sigma^-$ state. © *2003 American Institute of Physics.* [DOI: 10.1063/1.1623175]

Experimental methods for studying molecular photodissociation under collision-free conditions were introduced almost forty years ago.[1] Despite its importance in atmospheric and astrochemical processes,[2] no such studies have been reported for the hydroxyl radical. OH is experimentally challenging because all of the electronic transitions originating from $X\ ^2\Pi(v=0)$ lie in the vacuum ultraviolet region of the spectrum, except the well-known A-X transition used for laser induced fluorescence (LIF) detection. Furthermore, most sources of OH radicals also co-produce large amounts of $O(^3P)$ and $H(^2D)$ atoms, which can overwhelm the photoproduct signals. In this Communication, we report a photodissociation study of state-selected OD under collision-free conditions. Using a hexapole state selector and the velocity map imaging technique,[3,4] we measure angle–speed distributions for the $O(^3P_2)$ atom product following photodissociation at 226 nm and the $D(n=1, ^2S)$ product for photodissociation at 243 nm. New, fully *ab initio* calculations of the lower electronically excited states of OD were performed to yield accurate wave functions and internuclear dependent transition dipole functions for the states involved. These are used to explain the observed dissociation dynamics.

OD is produced by an electric discharge in a D_2O/Ar mixture expanded through a pulsed valve.[5] The molecular beam passes through a skimmer followed by a 12 cm long hexapole electrostatic lens which focuses OD in the $X\ ^2\Pi_{3/2}\ J=3/2,\ f$ lambda doublet level.[3] The enlargement of the distance between the source and photodissociation area by the insertion of the state selector decreases the contributions from all other species in the discharge beam, while the hexapole increases the concentration of the state-selected component by a factor of ~ 8 at the crossing point with the photodissociation laser. Using both laser induced fluorescence and resonance enhanced multiphoton ionization (REMPI) detection techniques,[6,7] the only species in the beam that was found to focus with the hexapole was OD. A corresponding increase in signal for the photodissociation processes with the hexapole on is thus direct proof that the photodissociation signal arises from OD.

At about 5 cm from the end of the hexapole both photodissociation of OD and photoionization of the atomic fragments is induced by pulsed radiation from a frequency-doubled dye laser with a pulse energy of ~ 1.5 mJ. The laser wavelength is chosen for two-photon resonant three-photon ionization [(2+1) REMPI] of either $O(^3P_2)$ atom products at 226 nm or $D(^2S)$ atom products at 243 nm. We will report comprehensive studies of $O(^3P_{2,1,0})$ detection from OD and OH at 226 nm in a later article. There are no known one- or two-photon transitions of OD or D_2O at these atomic REMPI wavelengths. The O^+ or D^+ atoms produced by the REMPI process are velocity mapped onto the two-dimensional imaging detector using an electrostatic inversion lens. A CCD camera records the 2-D image, which is presented as a slice through the reconstructed 3-D image using an inverse Abel transformation.[4]

Raw D^+ and O^+ images (hexapole on–hexapole off) are presented in Fig. 1. These images are a summation from 50 000 laser shots with the hexapole on, corrected by a subsequent background image taken with the hexapole off. Both the D^+ and O^+ images show a strong peak in the middle of the image, which corresponds to zero-velocity fragment $O(^3P_2)$ or $D(^2S)$ atoms formed in the discharge source. These atoms are not fully eliminated by the hexapole on–off subtraction scheme and cause a slight overload of the CCD camera at the image center. Signals at larger distances from the image center arise from atoms with increasingly higher photofragment velocities. The images are calibrated by $O(^3P_2)$ from O_2 photodissociation at 226 nm and by $D(^2S)$ from DI photodissociation at 243 nm. Two rings appear in the O^+ image corresponding to $O(^3P_2)$ atoms with velocity

a)Author to whom correspondence should be addressed. Electronic mail: parker@sci.kun.nl

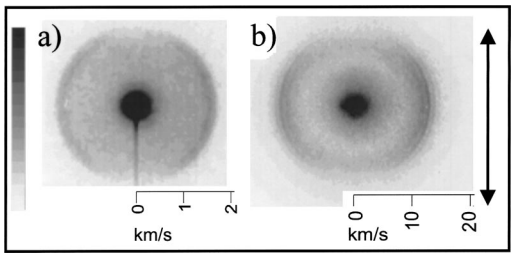

FIG. 1. Velocity map images of (a) O^+ and (b) D^+ ions detected following photodissociation of OD and subsequent 2+1 REMPI of the atomic products at 226 and 243 nm, respectively, with insets showing the velocity scale. Darker areas correspond to more signal, as coded by the gray-scale bar on the left side of the figure. The central spots originate from zero-velocity $O(^3P_2)$ or $D(^2S)$ atoms produced in the discharge source. The outer rings arise from photodissociation of vibrationally excited OD $X\,^2\Pi$ radicals. The arrow at the right indicates the direction of the laser polarization.

of 1670 and 1765 m/s with an uncertainty of ±25 m/s. Converting these O atom velocities to total kinetic energy release $[\mathrm{TKER}=(m_{\mathrm{OD}}/m_{\mathrm{D}})\times \mathrm{KER_O}]$ yields values of 2.08 and 2.32 ±0.06 eV. For D^+, at least three rings are seen, corresponding to D atom velocities of 11 800, 12 800, and 13 800 m/s and TKER values of 1.62, 1.91, and 2.21±0.06 eV, respectively. The TKER curves obtained from integrating over the angular distribution of the images are shown in Fig. 2. The widths of the peaks in the TKER curves are determined by electron recoil from the (2+1) REMPI process, as will be discussed in a future publication.

All of the observed angular distributions for D and O atom signals peak in the horizontal plane, indicating a perpendicular transition ($^2\Sigma^{+,-}\leftarrow{}^2\Pi$ or $^2\Delta\leftarrow{}^2\Pi$) to a rapidly dissociating state. For the stronger rings in the D atom image a fully perpendicular angular distribution is measured ($\sin^2\theta,\beta=-1.0\pm0.2$). A quantitative discussion of the angular distributions including the effects of O atom angular momentum alignment will be given in a following paper.

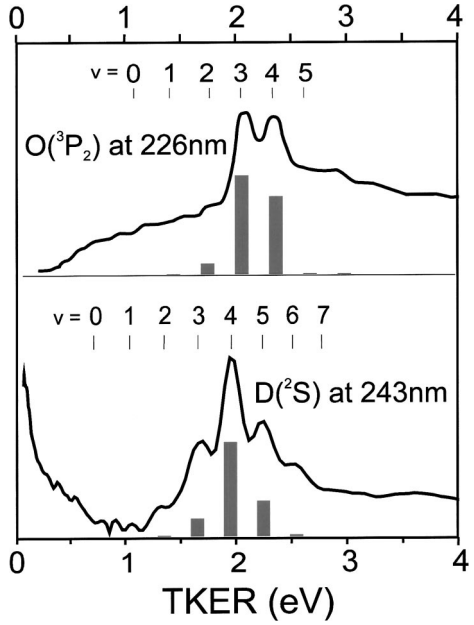

FIG. 2. Total kinetic energy release (TKER) derived from velocity map images of $O(^3P_2)$ and $D(^2S)$ fragment atoms following photodissociation of OD at 226 and 243 nm, respectively. The initial vibrational state of OD is determined from energy balance with $\mathrm{TKER}=h\nu+E(\mathrm{vib})_{\mathrm{OD}}-\mathrm{D}_0$. The bar graphs show the calculated photodissociation yields for OD $X\,^2\Pi(v)$ at a vibrational temperature of 1700 K.

The observed peaks in the TKER distributions can only be assigned to one-photon dissociation of OD in high vibrational levels of the ground $^2\Pi$ electronic state. Using the energy balance equation $\mathrm{TKER}=h\nu+E(\mathrm{vib})_{\mathrm{OD}}-\mathrm{D}_0$, with OD vibrational energies $E(\mathrm{vib})_{\mathrm{OD}}$ and bond energy D_0 from Refs. 8 and 9, the two main peaks seen for O atom detection at 226 nm are attributed to photodissociation of OD in $v=3$ and $v=4$, as marked in Fig. 2. For D atom detection at 243 nm, the three main peaks correspond to dissociation of OD ($v=3$, 4, and 5).

First principle calculations also demonstrate that the photodissociation processes at 226 and 243 nm occur by one-photon excitation of OD $X\,^2\Pi(v)$ to the repulsive $1\,^2\Sigma^-$ state. For these calculations, *ab initio* potentials for the $X\,^2\Pi$ and $1\,^2\Sigma^-$ states are computed at the MRCI level of theory with the MOLPRO package.[10–12] The aug-cc-pV6Z basis set[13] is used and the molecular orbitals are obtained from a CASSCF calculation[14,15] in which the lowest σ orbital is kept doubly occupied. The active space consists of four σ, two π_x, and two π_y orbitals. A grid of 30 points from 1 to 16 a_0 is employed. The quality of the $X\,^2\Pi$ potential was evaluated by computing the lowest seven vibrational energy levels using the sinc-function discrete variable representation method,[16] and the energy spacings were found to agree with experiment to within 0.1%. The R-dependent transition dipole moment between the two states was also calculated at the MRCI level with orbitals from a state-averaged CASSCF calculation. The photodissociation cross sections for OD at 226 and 243 nm were then evaluated using[17]

$$\sigma(E)=\frac{\pi\omega}{\varepsilon_0 c}\left|\langle X\,^2\Pi_x(v)|\mu_x(R)|1\,^2\Sigma^-,E^-\rangle\right|^2,$$

where $\hbar\omega$ is the photon energy and $|1\,^2\Sigma^-,E^-\rangle$ is the continuum wave function at total energy E with photodissociation boundary conditions,[18] which were obtained using the renormalized Numerov method.[17]

Figure 3 illustrates the process of photodissociation from the OD $X\,^2\Pi(v=5)$ state based on the calculated potentials, transition dipole function, and wave functions. As seen in the figure, when using 243 nm light OD($v=5$) can be excited to the $1\,^2\Sigma^-$ repulsive curve leading to the first dissociation limit, but poor overlap of the bound and continuum wave functions prevents absorption from OD($v=5$) at 226 nm. More quantitatively, the calculations show that the OD $X\,^2\Pi(v=5)$ photodissociation cross section is ~30 times larger at 243 nm than at 226 nm. This same effect is found experimentally, where a peak corresponding to $v=5$ is observed in the TKER curve for D atoms at 243 nm in Fig. 2, while this peak is not detectable above the background in the O atom TKER curve at 226 nm.

The relative intensity of the peaks in the TKER curves of Fig. 2 can be qualitatively understood based on the photodissociation cross sections computed for various vibrational states. The calculations predict that at a vibrational temperature of ~1700 K the $v=3$ and 4 states (and $v=2$ to a lesser

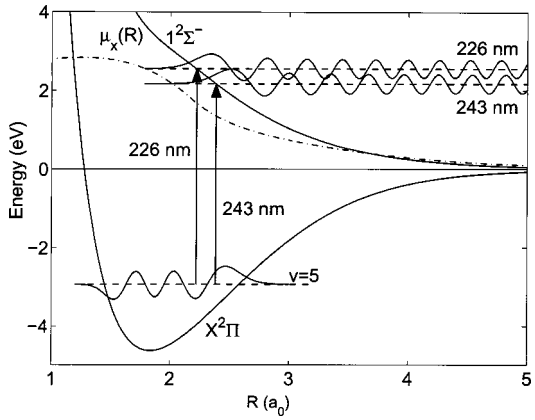

FIG. 3. Photodissociation of OD $X\,^2\Pi(v=5)$ at 226 and 243 nm via the repulsive $1\,^2\Sigma^-$ curve depicted with *ab initio* potentials, bound state and continuum wave functions, and transition dipole moment function (arbitrary units). The photodissociation cross section is large at 243 nm, but poor overlap of the wave functions when starting from $v=5$ results in minimal products at 226 nm, as seen experimentally.

extent) result in the largest photodissociation yield at 226 nm, while a distribution of states about $v=4$ (primarily $v=3$, 4, and 5) contribute to the yield at 243 nm. The predicted yields are shown in the bar graphs of Fig. 2. A Boltzmann population distribution in the vibrational states is assumed, and the temperature is adjusted to approximate the experimental TKER distributions. Note that such a temperature distribution is probably too simple for the description of the complicated excitation and cooling mechanisms in the pulsed discharge source. The quality of the experimental data is limited by problems in background subtraction and does not allow the extraction of a more accurate population distribution. A Boltzmann distribution of 1700 K for OD yields a fractional population in $v=5$, for example, of 3×10^{-5}. Independent measurement of the $v=1$ population in the molecular beam using laser induced fluorescence from the A-X transition yield a population of 4%, which agrees reasonably well with a 1700 K distribution. REMPI studies of OH via the $3\,^2\Sigma^-$ Rydberg state also detect population in higher vibrational levels of the ground electronic state from this discharge source, as will be described in a future publication.

In studies of other diatomic molecules, such as O_2 under similar conditions,[19] two-photon dissociation is often found to be the dominant channel. In this study, the laser intensity is suitable for two-photon resonant three-photon ionization of OH, O and H atoms. It is thus striking that the dominant signal is due to one-photon dissociation of OD to the repulsive $1\,^2\Sigma^-$ curve, starting from the very weakly populated higher vibrational levels of ground state OD. No evidence for two-photon dissociation is observed. While it is known that discharge beams produce vibrationally excited radicals,[20] it is remarkable that the imaging experiment is able to detect signal from vibrational levels which contain such small fractions (as low as 10^{-5}) of the population. Neither one-photon nor two-photon dissociation is detected from OD $X\,^2\Pi(v=0)$ at 243 or 226 nm. Stepwise two-photon dissociation via the repulsive $1\,^2\Sigma^-$ curve, starting from vibrationally excited OD is also not observed. The apparent weakness of two-photon excitation is most likely due to the transition dipole and unfavorable Franck–Condon overlap.

D.H.P. and M.I.L. thank the Dutch National Science Foundation (NWO) for a visiting professor fellowship B70-316. The experimental work in the Netherlands is part of the research program of the FOM-NWO organization. The *ab initio* work has been financially supported by the Council for Chemical Sciences of the Netherlands Organization for Scientific Research (CW-NWO). M.E.G. and M.I.L. gratefully acknowledge support from the Air Force Office of Scientific Research.

[1] *Molecular Photodissociation Dynamics*, edited by M. N. R. Ashfold and J. E. Baggott (Royal Society of Chemistry, London, 1987).
[2] *Progress in Atmospheric Physics*, edited by R. Rodrigo, J. J. López-Moreno, M. López-Puertas, and A. Molina (Kluwer Academic, Dordrecht, 1988).
[3] K. Schreel and J. J. ter Meulen, J. Phys. Chem. A **101**, 7639 (1997).
[4] A. T. J. B. Eppink and D. H. Parker, Rev. Sci. Instrum. **68**, 3477 (1997).
[5] M. C. van Beek and J. J. ter Meulen, Chem. Phys. Lett. **337**, 237 (2001).
[6] J. Luque and D. R. Crosley, "LIFBASE: Database and Spectral Simulation Program (Version 1.5)," SRI International Report No. MP 99-009 (1999).
[7] E. de Beer, M. P. Koopmans, C. A. De Lange, Y. Wang, and W. A. Chupka, J. Chem. Phys. **94**, 7634 (1991).
[8] M. C. Abrams, S. P. Davis, M. L. P. Rao, and R. Engleman, Jr., J. Mol. Spectrosc. **165**, 57 (1994).
[9] B. Ruscic, D. Feller, D. A. Dixon, K. A. Peterson, L. B. Harding, R. L. Asher, and A. F. Wagner, J. Phys. Chem. A **105**, 1 (2001).
[10] H.-J. Werner and P. J. Knowles, J. Chem. Phys. **89**, 5803 (1988).
[11] P. J. Knowles and H.-J. Werner, Chem. Phys. Lett. **145**, 514 (1988).
[12] MOLPRO is a package of *ab initio* programs written by H.-J. Werner and P. J. Knowles, with contributions from R. D. Amos, A. Berning, D. L. Cooper *et al.*
[13] T. H. Dunning, J. Chem. Phys. **90**, 1007 (1989).
[14] H.-J. Werner and P. J. Knowles, J. Chem. Phys. **82**, 5053 (1985).
[15] P. J. Knowles and H.-J. Werner, Chem. Phys. Lett. **115**, 259 (1985).
[16] G. C. Groenenboom and D. T. Colbert, J. Chem. Phys. **99**, 9681 (1993); D. T. Colbert and W. H. Miller, *ibid.* **96**, 1982 (1992).
[17] R. Schinke, *Photodissociation Dynamics* (Cambridge University Press, Cambridge, 1993).
[18] B. R. Johnson, NRCC Proceedings **5**, 86 (1979).
[19] B. Buijsse, W. J. van der Zande, A. T. J. B. Eppink, D. H. Parker, B. R. Lewis, and S. T. Gibson, J. Chem. Phys. **108**, 7229 (1998).
[20] G. B. Courreges-Lacoste, J. P. Sprengers, J. Bulthuis, S. Stolte, T. Motylewski, and H. Linnartz, Chem. Phys. Lett. **335**, 209 (2001).